

# Breaking black-hole uniqueness at supermassive scales

Astrid Eichhorn <sup>1,\*</sup> Pedro G. S. Fernandes <sup>1,†</sup> Aaron Held <sup>2,‡</sup> and Hector O. Silva <sup>3,§</sup>

<sup>1</sup>*CP3-Origins, University of Southern Denmark, Campusvej 55, DK-5230 Odense M, Denmark*

<sup>2</sup>*Institut de Physique Théorique Philippe Meyer,*

*Laboratoire de Physique de l'École normale supérieure (ENS), Université PSL,  
CNRS, Sorbonne Université, Université Paris Cité, F-75005 Paris, France*

<sup>3</sup>*Max Planck Institute for Gravitational Physics (Albert Einstein Institute), D-14476 Potsdam, Germany*

In general relativity, all vacuum black holes are described by the Kerr solution. Beyond general relativity, there is a prevailing expectation that deviations from the Kerr solution increase with the horizon curvature. We challenge this expectation by showing that, in a scalar-Gauss-Bonnet theory, black holes scalarize in a finite, adjustable window of black-hole masses, bounded from above and below. In this theory, there is an interplay between curvature scales and compactness, which we expect to protect neutron stars and other less compact objects from scalarization. In particular, black-hole uniqueness can be broken at supermassive black-hole scales, while solar-mass black holes remain well-described by the Kerr solution. To probe this scenario, observations targeting supermassive black holes are necessary.

**Introduction.** Our current best description of gravity, general relativity (GR), predicts that all vacuum black holes throughout the Universe, spanning a mass range of at least ten orders of magnitude, should be described by the Kerr metric [1]. This prediction of black-hole uniqueness is referred to as the “Kerr hypothesis” [2], and is supported by uniqueness [3, 4] and no-hair [5] theorems. Simultaneously, stringent constraints on modifications of GR arise from the outstanding agreement of its predictions with observations in the weak-field regime at solar-system scales [6]. This motivates us to explore modifications of GR that give rise to distinct gravitational phenomena exclusively in the strong-field regime. One such example is *scalarization* [7–15] – see Ref. [16] for a review – which is a strong-gravity phase transition endowing black holes and neutron stars with scalar hair.

Scalarization can be induced by coupling a real scalar field to the Gauss-Bonnet invariant,  $\mathcal{G} = R^2 - 4R_{\mu\nu}R^{\mu\nu} + R_{\mu\nu\alpha\beta}R^{\mu\nu\alpha\beta}$ . Through this coupling, the effective mass of scalar field fluctuations depends on  $\mathcal{G}$ , which can become tachyonically unstable around Kerr black holes, circumventing no-hair theorems [11]. The unstable GR black hole undergoes scalarization, settling into a new stationary, non-Kerr geometry, and thereby breaking black-hole uniqueness in certain regimes. Observations of black holes in the range of a few solar masses, conducted by the LIGO-Virgo-KAGRA (LVK) collaboration [17–19], binary pulsars [8, 20, 21], and other strong-field tests typically impose constraints on the length scale of new couplings at the order of kilometers [22–29]. In the conventional framework, scalarization is thus unattainable for black holes with intermediate and supermassive mass scales. Hence, the prevailing expectation is that black holes in these mass ranges should be well-described by the Kerr metric, even when solar-mass black holes are not [30].

In this Letter, we present a counterexample to this prevailing expectation. We introduce a model where black-hole uniqueness is maintained below a threshold

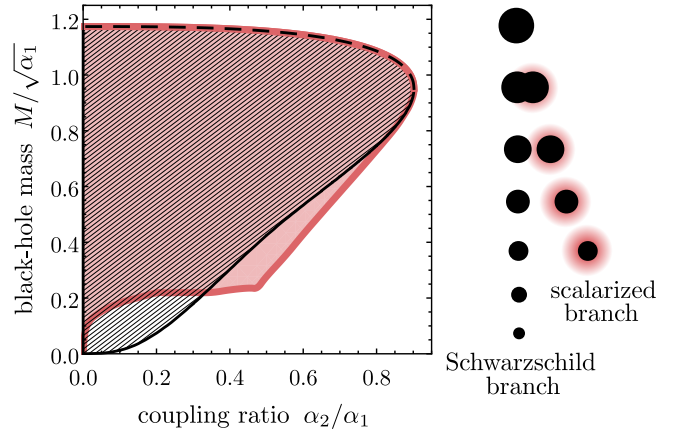


FIG. 1. Instability region of Schwarzschild spacetime (hatched region) and the region in which we find scalarized black holes (red shaded region) for the theory in Eq. (1). At the upper end of the mass window, the scalarized solution branches off the Schwarzschild branch continuously (as indicated by the dashed curve). At the lower end, there is no continuous transition between the two black-hole configurations.

value of the black-hole mass, but is violated above, as shown in Fig. 1. Moreover, our model incorporates a mechanism that prevents the scalarization of neutron stars, thus satisfying stringent constraints. Our findings carry significant implications as they suggest the potential existence of scalarized black holes across a spectrum of mass scales that can, for instance, be probed with the future Laser Interferometer Space Antenna (LISA) [31, 32], and with very-long-baseline-interferometry observations by the Event Horizon Telescope (EHT) collaboration [33–37].

**The model.** We consider the following action

$$S = \frac{1}{16\pi} \int d^4x \sqrt{-g} \left[ R - (\partial\phi)^2 + \alpha_1 F(\phi) \mathcal{G} - 2\alpha_2^3 F(\phi) \left( \psi \mathcal{G} - \frac{\psi^2}{2} \right) \right], \quad (1)$$

where  $\alpha_1$  and  $\alpha_2$  are coupling constants with dimensions of length squared [38], and  $\phi$  and  $\psi$  are real scalar fields. While  $\phi$  is dimensionless,  $\psi$  has the same dimension as the Gauss–Bonnet invariant  $\mathcal{G}$ , inverse length to the fourth. The equations of motion resulting from the action (1) are

$$G_{\mu\nu} = \partial_\mu \phi \partial_\nu \phi - \frac{1}{2} g_{\mu\nu} [(\partial\phi)^2 - \alpha_2^3 \psi^2 F(\phi)] - 4 {}^*R_{\mu\alpha\nu\beta}^* \nabla^\alpha \nabla^\beta [(-\alpha_1 + 2\alpha_2^3 \psi) F(\phi)], \quad (2)$$

$$\square\phi = \left[ -\alpha_1 \mathcal{G} + 2\alpha_2^3 \left( \psi \mathcal{G} - \frac{\psi^2}{2} \right) \right] \frac{F'(\phi)}{2}, \quad (3)$$

$$\psi - \mathcal{G} = 0, \quad (4)$$

where  ${}^*R_{\mu\alpha\nu\beta}^*$  is the double dual of the Riemann tensor. The equations of motion are manifestly second order, and thus our model belongs to a bi-scalar extension [39, 40] of Horndeski’s theory [41, 42]. The scalar  $\psi$  is not dynamical but, instead, acts as a Lagrange multiplier, such that the model is on-shell equivalent to one with a  $\mathcal{G}^2$  term in the equation of motion (3) for  $\phi$ . This also relates the model to a well-known class of modified theories of gravity known as “ $f(\mathcal{G})$  gravity” [43–46].

We require that the coupling function  $F(\phi)$  satisfies

$$F(0) = 0, \quad F'(0) = 0, \quad F''(0) > 0. \quad (5)$$

The first two conditions impose that vacuum solutions of GR are solutions of the theory, when the scalar field takes the constant value  $\phi = 0$  [47]. The third condition results in a tachyonic instability that we discuss in detail below. Without loss of generality, we assume  $F''(0) = 2$ . Other values of  $F''(0)$  can be absorbed into a redefinition of  $\alpha_1$  and  $\alpha_2$ . For small perturbations  $\delta\phi$  around  $\phi = 0$ , linearizing Eq. (3) leads to

$$(\square - \mu_{\text{eff}}^2) \delta\phi = 0, \quad \mu_{\text{eff}}^2(r) = -\alpha_1 \mathcal{G} + \alpha_2^3 \mathcal{G}^2, \quad (6)$$

where we have used the  $\psi$  equation of motion (4) and  $\mu_{\text{eff}}$  is the position-dependent effective mass of the perturbations. Scalarization is tied to a sufficiently negative squared effective mass, that can make the perturbations tachyonically unstable. The salient new feature of our proposal is already visible here: the effective mass is determined by a competition between two different terms. At sufficiently low curvature, the first term dominates and the theory behaves similarly to standard scalar–Gauss–Bonnet gravity [9–12]. At sufficiently high curvature, however, the second term dominates and, since it is always positive, prevents scalarization.

**(In)stability of the Schwarzschild black hole.** For now, we focus on a general static and spherically symmetric background metric

$$ds^2 = -a(r) dt^2 + b(r)^{-1} dr^2 + r^2(d\theta^2 + \sin^2\theta d\varphi^2), \quad (7)$$

which may describe either a black hole or the spacetime of a stellar object. The scalar-field perturbations can be separated as  $\delta\phi = u(r) \exp(-i\omega t) Y_{\ell m}(\theta, \varphi)/r$ , where  $Y_{\ell m}$  are the spherical harmonics. In terms of a radial coordinate  $dr_* = dr/\sqrt{ab}$ , the perturbation Eq. (6) takes a Schrödinger-like form

$$\frac{d^2 u}{dr_*^2} + (\omega^2 - V_{\text{eff}}) u = 0, \quad (8)$$

where the effective potential is

$$V_{\text{eff}}(r) = a(r) \left[ \frac{\ell(\ell+1)}{r^2} + \frac{1}{2ra} \frac{d(ab)}{dr} + \mu_{\text{eff}}^2 \right], \quad (9)$$

and where  $\mu_{\text{eff}}^2$  is given in Eq. (6). In this work we focus on monopolar perturbations, and thus set  $\ell = 0$ . For a Schwarzschild black hole, for which  $a = b = 1 - 2M/r$ , a sufficient condition for the existence of an unstable mode is [9, 48]  $\int_{-\infty}^{+\infty} V_{\text{eff}}(r_*) dr_* < 0$ . Heuristically, this condition, which would signal a bound state in quantum mechanics, is indicative of the existence of a mode with positive imaginary frequency, i.e., an exponentially growing perturbation. Computing the integral, this condition is equivalent to

$$1 - \frac{6}{5} \frac{\alpha_1}{M^2} + \frac{9}{22} \left( \frac{\alpha_2}{M^2} \right)^3 < 0, \quad (10)$$

where we used that  $\mathcal{G} = 48M^2/r^6$  in the Schwarzschild spacetime. When  $\alpha_2 = 0$ , we recover the usual Gauss–Bonnet scalarization result [9–12]. Instead, when  $0 < \alpha_2/\alpha_1 < \frac{4 \times 11^{1/3}}{5 \times 3^{2/3}} \approx 0.855$ , the inequality (10) is respected between two positive real values of  $M$ . There is thus a finite mass window, bounded from above and from below, within which the Schwarzschild solution must be unstable.

The inequality (10) is only a sufficient condition for instability. To conclusively establish instability, we use the S-deformation method [49–51]. For perturbations as in Eq. (8), this method establishes the linear stability of a black hole and amounts to showing that a smooth deformation function  $S(r)$  exists such that

$$\frac{dS}{dr} = \frac{S(r)^2 - V_{\text{eff}}(r)}{1 - 2M/r}. \quad (11)$$

For each choice of  $\alpha_1$ ,  $\alpha_2$  and  $M$ , we solve Eq. (11) numerically, imposing the boundary condition  $S(2M) = 0$ . Our results are presented in Fig. 1, where the hatched region shows the Schwarzschild instability region, where we could not find a deformation function. For each value  $\alpha_2/\alpha_1 > 0$ , this corresponds to a mass window bounded from above and below. We have also numerically solved the perturbation Eq. (8) in the Schwarzschild background, for a time-independent scalar (i.e., for  $\omega = 0$ ). We expected to find solutions if the scalarized branch connects continuously to the Schwarzschild branch; we were not able to find solutions to the perturbation equation for

masses near the lower bound of the mass range. Further, we found no solutions to the perturbation equation for values  $\alpha_2/\alpha_1 \gtrsim 0.902$ , indicating that scalarized black holes cease to exist past this value for the ratio of the couplings.

**Scalarized black holes.** We will now establish the existence of a new branch of scalarized solutions in the mass window where the Schwarzschild solution is unstable. For this, we work with the most general ansatz for a spherically symmetric, static metric, in isotropic coordinates,

$$ds^2 = -f\mathcal{N}^2 dt^2 + \frac{g}{f} (d\rho^2 + \rho^2 d\theta^2 + \rho^2 \sin^2 \theta d\varphi^2), \quad (12)$$

where  $\mathcal{N} = 1 - \rho_H/\rho$  and  $f$  and  $g$  are functions of  $\rho$ , with  $\rho_H$  the coordinate location of the event horizon. To construct the (numerical) scalarized solutions, we follow the approach of Ref. [52], using a publicly available code developed by one of us [53]. The numerical method, boundary conditions and validation of the code are discussed in the Supplemental Material. The Arnowitt-Deser-Misner (ADM) mass  $M$  follows from the asymptotic behavior of the metric function  $g_{tt} \sim -1 + 2M/\rho + \mathcal{O}(\rho^{-2})$ . The scalar  $\phi$  with scalar charge  $Q$  behaves as  $\phi \sim Q/\rho + \mathcal{O}(\rho^{-2})$  near spatial infinity. The entropy of the black hole does not follow the Bekenstein-Hawking relation [54, 55], but can be defined as an integral over the horizon [56, 57]

$$S = \frac{A_H}{4} + \frac{1}{4} \int_{\mathcal{H}} d^2x \sqrt{\gamma} (\alpha_1 - 2\alpha_2^3 \psi) F(\phi) \tilde{R}, \quad (13)$$

where  $\gamma$  is the determinant of the induced metric on the horizon  $\mathcal{H}$ ,  $\tilde{R}$  is its Ricci scalar, and  $A_H = 4\pi\rho_H^2 g/f|_{\mathcal{H}}$  is the area of the event horizon. To construct the numerical solutions, we chose the quadratic-exponential coupling commonly used in the literature [9, 12], which behaves quadratically around  $\phi = 0$ , is known to produce stable solutions in the scalar-Gauss-Bonnet model [58], and satisfies the conditions (5)

$$F(\phi) = \frac{1}{6} \left( 1 - e^{-6\phi^2} \right). \quad (14)$$

We have confirmed that for each nonzero value of  $\alpha_2/\alpha_1$ , scalarized solutions exist only within a mass window bounded from above and below, as shown in Fig. 1, where the red shaded region denotes the domain of existence of scalarized black holes for each coupling ratio  $\alpha_2/\alpha_1$ . While the bifurcation points from the Schwarzschild solution were notably in agreement with the upper bound S-deformation predictions, the termination point of the scalarized black hole branch differed, in general. In particular, for couplings obeying  $\alpha_2/\alpha_1 \lesssim 0.3$ , the endpoint of the scalarized branches occurs for values of the mass higher than those obtained with the S-deformation method. This suggests a mass range where stable, spherically symmetric and static black hole solutions are entirely absent. On

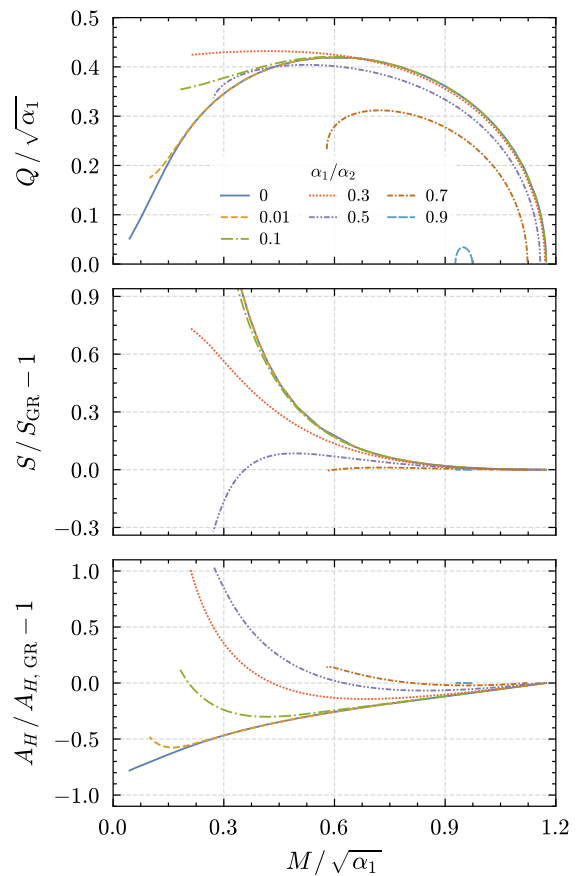


FIG. 2. Scalar charge (upper panel), entropy (middle panel), and horizon area (lower panel) of the scalarized solutions as functions of  $M/\sqrt{\alpha_1}$ . The scalar charge is normalized to the value of the coupling, while the entropy and horizon area are compared with those of a Schwarzschild black hole with the same mass.

the other hand, for higher  $\alpha_2/\alpha_1$  the scalarized branch ends for masses smaller than those obtained with the S-deformation method, leading to a mass range where stable Schwarzschild black holes and scalarized black holes co-exist. As we approach the maximum value  $\alpha_2/\alpha_1 \approx 0.902$ , the endpoint of the scalarized branches also approach the lower-bound values obtained with the S-deformation method. In contrast to typical scenarios in standard scalar-Gauss-Bonnet gravity, where branches terminate in singular solutions [27], we detect no singular behavior in the solutions when inspecting the Ricci and Gauss-Bonnet scalars at the black hole horizon. Instead, we observe a decline in the accuracy of the scalarized solutions as we approach the end of the scalarized branch, and at a certain point, the code ceases to converge to a scalarized solution. Past this point, our numerical method only finds Schwarzschild black holes. We hypothesize that this is connected to an overall diminishingly negative effective mass squared entering the scalar field equation as  $M/\sqrt{\alpha_1}$  decreases, as observed in our numerical analysis.

Beyond a certain threshold, the negative contributions to the scalar field equation seem insufficient to support the existence of a scalarized black hole.

As shown in Fig. 2, the entropy of the scalarized solution is greater than that of a corresponding Schwarzschild black hole, except in proximity to the termination of the existence domain in certain instances, such as for  $\alpha_2/\alpha_1 = 0.5$  and  $\alpha_2/\alpha_1 = 0.7$ . This trend signifies an entropic preference for scalarized solutions in most cases. Notably, the physical quantities exhibit non-monotonic deviations from those of GR, with regions where they are both smaller and larger. This is evident, for instance, in the variation of the horizon area as shown in Fig. 2. The scalar charge  $Q$  normalized to the length scale  $\sqrt{\alpha_1}$  is also shown in Fig. 2. Plots for other physical quantities of interest in astrophysical contexts are shown in the Supplemental Material.

**Scalarization in neutron stars and other less compact objects.** We do not, in general, expect scalarization to occur in neutron stars or other stellar objects. Using the Tolman-Oppenheimer-Volkoff (TOV) equations [59, 60], the Gauss-Bonnet invariant of a star described by the metric (7) can be expressed as [11, 61]:

$$\mathcal{G} = \frac{48m^2}{r^6} - \frac{128\pi(m + 2\pi r^3 p)\varepsilon}{r^3}, \quad (15)$$

where  $m = r(1 - b)/2$  is the mass function, and  $p$  and  $\varepsilon$  are the pressure and energy density inside the star, respectively. At the surface, the energy density becomes zero, and  $m$  becomes constant and equal to the ADM mass  $M$ . The Gauss-Bonnet invariant smoothly connects with that of the Schwarzschild metric, while being predominantly negative in the interior of the star [11]. Hence, in our context, an instability could only be triggered at the outer region of the star or in its exterior.

We have solved the TOV equations for a neutron star model with  $M = 1.4 M_\odot$ , employing the AP4 equation of state [62]. In Fig. 3, we plot the effective potential (9) for scalar perturbations around this neutron star solution, considering various values of  $\alpha_2/\alpha_1$  and assuming  $\sqrt{\alpha_1} \approx 10^6 M_\odot$ . With increasing  $\alpha_2/\alpha_1$ , the negative regions in the effective potential become progressively weaker and shift further away from the surface of the neutron star. The effective potential within the star is overwhelmingly positive if  $\alpha_2 \neq 0$ . Consequently, we expect that scalarization of neutron stars can be avoided, at least if both couplings are sufficiently large, i.e.,  $\alpha_1 \gg M_\odot$  and  $\alpha_2 \gg M_\odot$ .

Defining the compactness of a body with ADM mass  $M$  and radius  $r_s$  as  $C = 2M/r_s$ , the effective potential in Eq. (9) is proportional to an overall factor of  $C^3$  in the

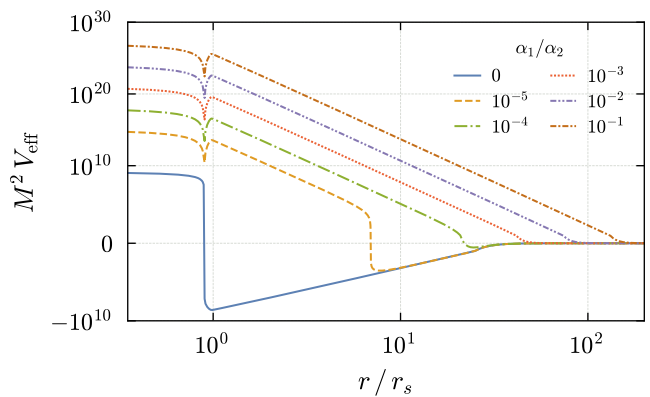


FIG. 3. The dimensionless effective potential  $M^2 V_{\text{eff}}$  for scalar perturbations around a neutron star with  $M \approx 1.4 M_\odot$  and radius  $r_s \approx 11$  km, described by the AP4 equation of state [62], considering various values of  $\alpha_2/\alpha_1$  and assuming  $\sqrt{\alpha_1} \approx 10^6 M_\odot$ .

exterior region ( $r \geq r_s$ ) where the metric is Schwarzschild

$$M^2 V_{\text{eff}} = \frac{1}{4} C^3 \frac{(r/r_s - C)}{(r/r_s)^4} \left[ 1 - 2\sqrt{3}\alpha_1\sqrt{\mathcal{G}} + 2\sqrt{3}(\alpha_2\sqrt{\mathcal{G}})^3 \right]. \quad (16)$$

We observe that when two objects possess different masses, but their Gauss-Bonnet curvature near the surface is of the same order of magnitude, the effective potential of the less compact object is suppressed by a factor of  $C^3$ . This suppression makes it more challenging for the less compact object to undergo scalarization. Therefore, astrophysical bodies like the Sun (for which  $C \sim 10^{-6}$ ), exhibit an extremely weak effective potential near their surface, even if black holes (for which  $C = 1$ ) with the same surface Gauss-Bonnet curvature are scalarized. Consequently, we do not anticipate scalarization to occur, for instance, within the solar system. Similarly, we do not expect that laboratory experiments which are sensitive to curvatures of the same order as the horizon curvature of a supermassive black hole, can probe the scalarized regime. The weak negative regions that could potentially exist in  $V_{\text{eff}}$  for less compact objects may, moreover, be partially or entirely eliminated by adding a small explicit mass term for the scalar  $\phi$  to the action in Eq. (1).

**Conclusions and outlook.** There is a widely accepted expectation that, if the Kerr hypothesis breaks down, it does so above a critical curvature threshold. We present the first paradigmatic example of a theory in which this expectation does not hold true, because black-hole uniqueness is broken – and the Schwarzschild solution is unstable – in a *finite* and bounded window of horizon curvature, or, equivalently, black-hole mass. This window depends on the two coupling constants  $\alpha_1$  and  $\alpha_2$  in the action. If both coupling constants are of the same order of magnitude and there is no hierarchy of length scales, the



window is narrow and targets a specific black-hole mass scale  $M \sim \sqrt{\alpha_1} \sim \sqrt{\alpha_2}$ . Conversely, it is necessary to introduce a hierarchy of scales into the theory in order to obtain an expansive window. Dependent on the value of  $\alpha_1 \sim \alpha_2$ , different observational channels can constrain the theory.

First, if the mass window lies within the solar-mass range, our theory can be constrained by LVK observations [17–19]. For instance, an equal-mass binary may start out as a binary of two Schwarzschild black holes, but end up in the mass window in which the merger remnant may be scalarized. This is in contrast to other scalarization scenarios in the literature and could lead to a detectable mismatch between the expected and the observed post-merger phase of the gravitational-wave signal [63, 64].

Second, if  $\alpha_2$  and  $\alpha_1$  are such that solar-mass black holes are described by the Schwarzschild solution, but supermassive black holes are not, LVK observations are insensitive to the modification of GR and observations of supermassive black holes constitute the only pathway to constrain the theory. We expect that this can already be constrained from existing EHT observations [33–36] and will address this in future work. Given the factor of roughly  $10^3$  between the mass of Sgr A\* and M87\*, it may well be that only one of them is scalarized, because a hierarchy between  $\alpha_1$  and  $\alpha_2$  must be introduced in order to scalarize both. Future upgrades of the EHT [37, 65] and planned space-based gravitational-wave observatories like LISA [31, 32], TianQin [66] or Taiji [67] may also probe the theory. As a first step in this direction, one may focus on extreme-mass-ratio-inspirals (EMRIs), in which a small (nonscalarized) black hole orbits a large (scalarized) black hole because EMRIs are an important observational target for LISA. Another possibility, is to analyze the coalescence of massive black-hole binaries, which may be detected by LISA with signal-to-noise ratio reaching thousands [68–70]. To determine whether stellar orbits and gas dynamics near supermassive black holes [71–74] as well as x-ray observations [75, 76] also provide constraints, one should characterize deviations in the post-Newtonian expansion. If supermassive black holes surpass the instability threshold due to accretion, the resulting spontaneous transition may also result in observable signatures [77, 78]. In addition, the stochastic gravitational-wave background from a population of supermassive black holes may be modified by scalarization and affect pulsar-timing-array data [79–84].

As  $\alpha_2/\alpha_1$  decreases, the window widens (see Fig. 1) and the theory may be constrained at various black-hole mass scales. Moreover, we find indications for a mass gap, i.e., a range of black-hole masses for which no stable branch of spherically symmetric and stationary solutions exists. To further understand the different black-hole branches and understand whether the mass gap persists beyond spherical symmetry, we plan to study rotating black-hole

solutions. At nonzero spin, minimally and nonminimally coupled scalar fields can trigger new instabilities due to superradiance [85, 86] and spin-induced scalarization [13–15].

Finally, the upper curvature bound may even be taken to cosmological scales. The present theory might provide a screening mechanism which hides cosmological modifications from solar-system (and even galactic) observations, see, e.g., [87] for review. The latter application assumes that our results on black-hole (non)uniqueness carry over to cosmological spacetimes. This motivates us to generalize the presented paradigmatic example to a larger class of theories. We expect that theories with several scalars and distinct effective masses may exhibit similar effects.

**Acknowledgements.** AE and PGSF are supported by a grant (29405) from VILLUM fonden. HOS acknowledges funding from the Deutsche Forschungsgemeinschaft (DFG) - Project No.: 386119226.

---

\* eichhorn@sdu.dk

† pgsfernandes@sdu.dk

‡ aaron.held@phys.ens.fr

§ hector.silva@aei.mpg.de

- [1] R. P. Kerr, Gravitational field of a spinning mass as an example of algebraically special metrics, *Phys. Rev. Lett.* **11**, 237 (1963).
- [2] C. A. R. Herdeiro, Black Holes: On the Universality of the Kerr Hypothesis, *Lect. Notes Phys.* **1017**, 315 (2023), [arXiv:2204.05640 \[gr-qc\]](#).
- [3] B. Carter, Axisymmetric black hole has only two degrees of freedom, *Phys. Rev. Lett.* **26**, 331 (1971).
- [4] D. C. Robinson, Uniqueness of the kerr black hole, *Phys. Rev. Lett.* **34**, 905 (1975).
- [5] C. A. R. Herdeiro and E. Radu, Asymptotically flat black holes with scalar hair: a review, *Int. J. Mod. Phys. D* **24**, 1542014 (2015), [arXiv:1504.08209 \[gr-qc\]](#).
- [6] C. M. Will, The Confrontation between General Relativity and Experiment, *Living Rev. Rel.* **17**, 4 (2014), [arXiv:1403.7377 \[gr-qc\]](#).
- [7] T. Damour and G. Esposito-Farèse, Nonperturbative strong-field effects in tensor-scalar theories of gravitation, *Phys. Rev. Lett.* **70**, 2220 (1993).
- [8] T. Damour and G. Esposito-Farèse, Tensor-scalar gravity and binary pulsar experiments, *Phys. Rev. D* **54**, 1474 (1996), [arXiv:gr-qc/9602056](#).
- [9] D. D. Doneva and S. S. Yazadjiev, New Gauss-Bonnet Black Holes with Curvature-Induced Scalarization in Extended Scalar-Tensor Theories, *Phys. Rev. Lett.* **120**, 1311103 (2018), [arXiv:1711.01187 \[gr-qc\]](#).
- [10] G. Antoniou, A. Bakopoulos, and P. Kanti, Evasion of No-Hair Theorems and Novel Black-Hole Solutions in Gauss-Bonnet Theories, *Phys. Rev. Lett.* **120**, 1311102 (2018), [arXiv:1711.03390 \[hep-th\]](#).
- [11] H. O. Silva, J. Sakstein, L. Gualtieri, T. P. Sotiriou, and E. Berti, Spontaneous scalarization of black holes and compact stars from a Gauss-Bonnet coupling, *Phys. Rev. Lett.* **120**, 1311104 (2018), [arXiv:1711.02080 \[gr-qc\]](#).
- [12] P. V. P. Cunha, C. A. R. Herdeiro, and E. Radu, Sponta-

- neously Scalarized Kerr Black Holes in Extended Scalar-Tensor–Gauss-Bonnet Gravity, *Phys. Rev. Lett.* **123**, 011101 (2019), [arXiv:1904.09997 \[gr-qc\]](#).
- [13] A. Dima, E. Barausse, N. Franchini, and T. P. Sotiriou, Spin-induced black hole spontaneous scalarization, *Phys. Rev. Lett.* **125**, 231101 (2020), [arXiv:2006.03095 \[gr-qc\]](#).
- [14] C. A. R. Herdeiro, E. Radu, H. O. Silva, T. P. Sotiriou, and N. Yunes, Spin-induced scalarized black holes, *Phys. Rev. Lett.* **126**, 011103 (2021), [arXiv:2009.03904 \[gr-qc\]](#).
- [15] E. Berti, L. G. Collodel, B. Kleihaus, and J. Kunz, Spin-induced black-hole scalarization in Einstein-scalar-Gauss-Bonnet theory, *Phys. Rev. Lett.* **126**, 011104 (2021), [arXiv:2009.03905 \[gr-qc\]](#).
- [16] D. D. Doneva, F. M. Ramazanoğlu, H. O. Silva, T. P. Sotiriou, and S. S. Yazadjiev, Scalarization (2022), [arXiv:2211.01766 \[gr-qc\]](#).
- [17] B. P. Abbott *et al.* (LIGO Scientific, Virgo), Observation of Gravitational Waves from a Binary Black Hole Merger, *Phys. Rev. Lett.* **116**, 061102 (2016), [arXiv:1602.03837 \[gr-qc\]](#).
- [18] B. P. Abbott *et al.* (LIGO Scientific, Virgo), GW170817: Observation of Gravitational Waves from a Binary Neutron Star Inspiral, *Phys. Rev. Lett.* **119**, 161101 (2017), [arXiv:1710.05832 \[gr-qc\]](#).
- [19] B. P. Abbott *et al.* (LIGO Scientific, Virgo), GWTC-1: A Gravitational-Wave Transient Catalog of Compact Binary Mergers Observed by LIGO and Virgo during the First and Second Observing Runs, *Phys. Rev. X* **9**, 031040 (2019), [arXiv:1811.12907 \[astro-ph.HE\]](#).
- [20] N. Yunes and X. Siemens, Gravitational-Wave Tests of General Relativity with Ground-Based Detectors and Pulsar Timing-Arrays, *Living Rev. Rel.* **16**, 9 (2013), [arXiv:1304.3473 \[gr-qc\]](#).
- [21] B. C. Seymour and K. Yagi, Testing General Relativity with Black Hole-Pulsar Binaries, *Phys. Rev. D* **98**, 124007 (2018), [arXiv:1808.00080 \[gr-qc\]](#).
- [22] R. Nair, S. Perkins, H. O. Silva, and N. Yunes, Fundamental Physics Implications for Higher-Curvature Theories from Binary Black Hole Signals in the LIGO-Virgo Catalog GWTC-1, *Phys. Rev. Lett.* **123**, 191101 (2019), [arXiv:1905.00870 \[gr-qc\]](#).
- [23] S. E. Perkins, R. Nair, H. O. Silva, and N. Yunes, Improved gravitational-wave constraints on higher-order curvature theories of gravity, *Phys. Rev. D* **104**, 024060 (2021), [arXiv:2104.11189 \[gr-qc\]](#).
- [24] K. Yamada, T. Narikawa, and T. Tanaka, Testing massive-field modifications of gravity via gravitational waves, *PTEP* **2019**, 103E01 (2019), [arXiv:1905.11859 \[gr-qc\]](#).
- [25] H.-T. Wang, S.-P. Tang, P.-C. Li, M.-Z. Han, and Y.-Z. Fan, Tight constraints on Einstein-dilation-Gauss-Bonnet gravity from GW190412 and GW190814, *Phys. Rev. D* **104**, 024015 (2021), [arXiv:2104.07590 \[gr-qc\]](#).
- [26] Z. Lyu, N. Jiang, and K. Yagi, Constraints on Einstein-dilation-Gauss-Bonnet gravity from black hole-neutron star gravitational wave events, *Phys. Rev. D* **105**, 064001 (2022), [Erratum: *Phys.Rev.D* 106, 069901 (2022), Erratum: *Phys.Rev.D* 106, 069901 (2022)], [arXiv:2201.02543 \[gr-qc\]](#).
- [27] P. G. S. Fernandes, D. J. Mulryne, and J. F. M. Delgado, Exploring the small mass limit of stationary black holes in theories with Gauss–Bonnet terms, *Class. Quant. Grav.* **39**, 235015 (2022), [arXiv:2207.10692 \[gr-qc\]](#).
- [28] G. Ventagli, G. Antoniou, A. Lehébel, and T. P. Sotiriou, Neutron star scalarization with Gauss-Bonnet and Ricci scalar couplings, *Phys. Rev. D* **104**, 124078 (2021), [arXiv:2111.03644 \[gr-qc\]](#).
- [29] V. I. Danchev, D. D. Doneva, and S. S. Yazadjiev, Constraining scalarization in scalar-Gauss-Bonnet gravity through binary pulsars, *Phys. Rev. D* **106**, 124001 (2022), [arXiv:2112.03869 \[gr-qc\]](#).
- [30] G. D’Addario, A. Padilla, P. M. Saffin, T. P. Sotiriou, and A. Spiers, Ringdowns for black holes with scalar hair: the large mass case (2023), [arXiv:2311.17666 \[gr-qc\]](#).
- [31] P. Amaro-Seoane, H. Audley, S. Babak, J. Baker, E. Barausse, P. Bender, E. Berti, P. Binetruy, M. Born, D. Borzoluzzi, *et al.*, Laser interferometer space antenna, arXiv preprint [arXiv:1702.00786](#) (2017).
- [32] E. Barausse *et al.*, Prospects for Fundamental Physics with LISA, *Gen. Rel. Grav.* **52**, 81 (2020), [arXiv:2001.09793 \[gr-qc\]](#).
- [33] K. Akiyama *et al.* (Event Horizon Telescope), First M87 Event Horizon Telescope Results. VI. The Shadow and Mass of the Central Black Hole, *Astrophys. J. Lett.* **875**, L6 (2019), [arXiv:1906.11243 \[astro-ph.GA\]](#).
- [34] D. Psaltis *et al.* (Event Horizon Telescope), Gravitational Test Beyond the First Post-Newtonian Order with the Shadow of the M87 Black Hole, *Phys. Rev. Lett.* **125**, 141104 (2020), [arXiv:2010.01055 \[gr-qc\]](#).
- [35] P. Kocherlakota *et al.* (Event Horizon Telescope), Constraints on black-hole charges with the 2017 EHT observations of M87\*, *Phys. Rev. D* **103**, 104047 (2021), [arXiv:2105.09343 \[gr-qc\]](#).
- [36] K. Akiyama *et al.* (Event Horizon Telescope), First Sagittarius A\* Event Horizon Telescope Results. VI. Testing the Black Hole Metric, *Astrophys. J. Lett.* **930**, L17 (2022).
- [37] D. Ayzenberg *et al.*, Fundamental Physics Opportunities with the Next-Generation Event Horizon Telescope (2023), [arXiv:2312.02130 \[astro-ph.HE\]](#).
- [38] We work in units in which  $G = c = 1$ .
- [39] S. Ohashi, N. Tanahashi, T. Kobayashi, and M. Yamaguchi, The most general second-order field equations of bi-scalar-tensor theory in four dimensions, *JHEP* **07**, 008, [arXiv:1505.06029 \[gr-qc\]](#).
- [40] C. Charmousis, T. Kolyvaris, E. Papantonopoulos, and M. Tsoukalas, Black Holes in Bi-scalar Extensions of Horndeski Theories, *JHEP* **07**, 085, [arXiv:1404.1024 \[gr-qc\]](#).
- [41] G. W. Horndeski, Second-order scalar-tensor field equations in a four-dimensional space, *Int. J. Theor. Phys.* **10**, 363 (1974).
- [42] T. Kobayashi, Horndeski theory and beyond: a review, *Rept. Prog. Phys.* **82**, 086901 (2019), [arXiv:1901.07183 \[gr-qc\]](#).
- [43] S. Nojiri and S. D. Odintsov, Modified Gauss-Bonnet theory as gravitational alternative for dark energy, *Phys. Lett. B* **631**, 1 (2005), [arXiv:hep-th/0508049](#).
- [44] B. Li, J. D. Barrow, and D. F. Mota, The Cosmology of Modified Gauss-Bonnet Gravity, *Phys. Rev. D* **76**, 044027 (2007), [arXiv:0705.3795 \[gr-qc\]](#).
- [45] A. De Felice and S. Tsujikawa, Construction of cosmologically viable  $f(G)$  dark energy models, *Phys. Lett. B* **675**, 1 (2009), [arXiv:0810.5712 \[hep-th\]](#).
- [46] S.-Y. Zhou, E. J. Copeland, and P. M. Saffin, Cosmological Constraints on  $f(G)$  Dark Energy Models, *JCAP* **07**, 009, [arXiv:0903.4610 \[gr-qc\]](#).
- [47] Contrary to standard scalar-Gauss–Bonnet gravity, we no longer have the symmetry  $F(\phi) \rightarrow F(\phi) + c$ , for constant

- c.
- [48] W. F. Buell and B. A. Shadwick, Potentials and bound states, *American Journal of Physics* **63**, 256 (1995).
- [49] M. Kimura, A simple test for stability of black hole by  $S$ -deformation, *Class. Quant. Grav.* **34**, 235007 (2017), [arXiv:1706.01447 \[gr-qc\]](https://arxiv.org/abs/1706.01447).
- [50] M. Kimura and T. Tanaka, Robustness of the  $S$ -deformation method for black hole stability analysis, *Class. Quant. Grav.* **35**, 195008 (2018), [arXiv:1805.08625 \[gr-qc\]](https://arxiv.org/abs/1805.08625).
- [51] M. Kimura and T. Tanaka, Stability analysis of black holes by the  $S$ -deformation method for coupled systems, *Class. Quant. Grav.* **36**, 055005 (2019), [arXiv:1809.00795 \[gr-qc\]](https://arxiv.org/abs/1809.00795).
- [52] P. G. S. Fernandes and D. J. Mulryne, A new approach and code for spinning black holes in modified gravity, *Class. Quant. Grav.* **40**, 165001 (2023), [arXiv:2212.07293 \[gr-qc\]](https://arxiv.org/abs/2212.07293).
- [53] P. G. S. Fernandes, SpinningBlackHoles.jl, <https://github.com/pgsfernandes/SpinningBlackHoles.jl>.
- [54] J. D. Bekenstein, Black holes and entropy, *Phys. Rev. D* **7**, 2333 (1973).
- [55] J. D. Bekenstein, Generalized second law of thermodynamics in black-hole physics, *Phys. Rev. D* **9**, 3292 (1974).
- [56] R. M. Wald, Black hole entropy is the Noether charge, *Phys. Rev. D* **48**, R3427 (1993), [arXiv:gr-qc/9307038](https://arxiv.org/abs/gr-qc/9307038).
- [57] V. Iyer and R. M. Wald, Some properties of Noether charge and a proposal for dynamical black hole entropy, *Phys. Rev. D* **50**, 846 (1994), [arXiv:gr-qc/9403028](https://arxiv.org/abs/gr-qc/9403028).
- [58] H. O. Silva, C. F. B. Macedo, T. P. Sotiriou, L. Gualtieri, J. Sakstein, and E. Berti, Stability of scalarized black hole solutions in scalar-Gauss-Bonnet gravity, *Phys. Rev. D* **99**, 064011 (2019), [arXiv:1812.05590 \[gr-qc\]](https://arxiv.org/abs/1812.05590).
- [59] J. R. Oppenheimer and G. M. Volkoff, On massive neutron cores, *Phys. Rev.* **55**, 374 (1939).
- [60] R. C. Tolman, Static solutions of Einstein's field equations for spheres of fluid, *Phys. Rev.* **55**, 364 (1939).
- [61] D. D. Doneva and S. S. Yazadjiev, Neutron star solutions with curvature induced scalarization in the extended Gauss-Bonnet scalar-tensor theories, *JCAP* **04**, 011, [arXiv:1712.03715 \[gr-qc\]](https://arxiv.org/abs/1712.03715).
- [62] A. Akmal, V. R. Pandharipande, and D. G. Ravenhall, The Equation of state of nucleon matter and neutron star structure, *Phys. Rev. C* **58**, 1804 (1998), [arXiv:nuc-th/9804027](https://arxiv.org/abs/nuc-th/9804027).
- [63] M. Elley, H. O. Silva, H. Witek, and N. Yunes, Spin-induced dynamical scalarization, descalarization, and stealthness in scalar-Gauss-Bonnet gravity during a black hole coalescence, *Phys. Rev. D* **106**, 044018 (2022), [arXiv:2205.06240 \[gr-qc\]](https://arxiv.org/abs/2205.06240).
- [64] D. D. Doneva, L. Aresté Saló, K. Clough, P. Figueras, and S. S. Yazadjiev, Testing the limits of scalar-Gauss-Bonnet gravity through nonlinear evolutions of spin-induced scalarization, *Phys. Rev. D* **108**, 084017 (2023), [arXiv:2307.06474 \[gr-qc\]](https://arxiv.org/abs/2307.06474).
- [65] M. D. Johnson *et al.*, Key Science Goals for the Next-Generation Event Horizon Telescope, *Galaxies* **11**, 61 (2023), [arXiv:2304.11188 \[astro-ph.HE\]](https://arxiv.org/abs/2304.11188).
- [66] J. Luo *et al.* (TianQin), TianQin: a space-borne gravitational wave detector, *Class. Quant. Grav.* **33**, 035010 (2016), [arXiv:1512.02076 \[astro-ph.IM\]](https://arxiv.org/abs/1512.02076).
- [67] W.-R. Hu and Y.-L. Wu, The Taiji Program in Space for gravitational wave physics and the nature of gravity, *Natl. Sci. Rev.* **4**, 685 (2017).
- [68] E. Berti, V. Cardoso, and C. M. Will, On gravitational-wave spectroscopy of massive black holes with the space interferometer LISA, *Phys. Rev. D* **73**, 064030 (2006), [arXiv:gr-qc/0512160](https://arxiv.org/abs/gr-qc/0512160).
- [69] A. Klein *et al.*, Science with the space-based interferometer eLISA: Supermassive black hole binaries, *Phys. Rev. D* **93**, 024003 (2016), [arXiv:1511.05581 \[gr-qc\]](https://arxiv.org/abs/1511.05581).
- [70] S. Bhagwat, C. Pacilio, E. Barausse, and P. Pani, Landscape of massive black-hole spectroscopy with LISA and the Einstein Telescope, *Phys. Rev. D* **105**, 124063 (2022), [arXiv:2201.00023 \[gr-qc\]](https://arxiv.org/abs/2201.00023).
- [71] A. M. Ghez *et al.*, Measuring Distance and Properties of the Milky Way's Central Supermassive Black Hole with Stellar Orbits, *Astrophys. J.* **689**, 1044 (2008), [arXiv:0808.2870 \[astro-ph\]](https://arxiv.org/abs/0808.2870).
- [72] GRAVITY Collaboration *et al.*, Detection of orbital motions near the last stable circular orbit of the massive black hole SgrA\*, *Astronomy & Astrophysics* **618**, L10 (2018), [arXiv:1810.12641 \[astro-ph.GA\]](https://arxiv.org/abs/1810.12641).
- [73] T. Do *et al.*, Relativistic redshift of the star S0-2 orbiting the Galactic center supermassive black hole, *Science* **365**, 664 (2019), [arXiv:1907.10731 \[astro-ph.GA\]](https://arxiv.org/abs/1907.10731).
- [74] A. Foschi *et al.* (GRAVITY), Using the motion of S2 to constrain scalar clouds around Sgr A\*, *Mon. Not. Roy. Astron. Soc.* **524**, 1075 (2023), [arXiv:2306.17215 \[astro-ph.GA\]](https://arxiv.org/abs/2306.17215).
- [75] C. Bambi, A. Cardenas-Avendano, T. Dauser, J. A. Garcia, and S. Nampalliwar, Testing the Kerr black hole hypothesis using X-ray reflection spectroscopy, *Astrophys. J.* **842**, 76 (2017), [arXiv:1607.00596 \[gr-qc\]](https://arxiv.org/abs/1607.00596).
- [76] C. Bambi, Testing Gravity with Black Hole X-Ray Data, (2022), [arXiv:2210.05322 \[gr-qc\]](https://arxiv.org/abs/2210.05322).
- [77] P. G. S. Fernandes, C. A. R. Herdeiro, A. M. Pombo, E. Radu, and N. Sanchis-Gual, Spontaneous Scalarisation of Charged Black Holes: Coupling Dependence and Dynamical Features, *Class. Quant. Grav.* **36**, 134002 (2019), [Erratum: *Class. Quant. Grav.* **37**, 049501 (2020)], [arXiv:1902.05079 \[gr-qc\]](https://arxiv.org/abs/1902.05079).
- [78] P. G. S. Fernandes, C. A. R. Herdeiro, A. M. Pombo, E. Radu, and N. Sanchis-Gual, Charged black holes with axionic-type couplings: Classes of solutions and dynamical scalarization, *Phys. Rev. D* **100**, 084045 (2019), [arXiv:1908.00037 \[gr-qc\]](https://arxiv.org/abs/1908.00037).
- [79] G. Agazie *et al.* (NANOGrav), The NANOGrav 15 yr Data Set: Evidence for a Gravitational-wave Background, *Astrophys. J. Lett.* **951**, L8 (2023), [arXiv:2306.16213 \[astro-ph.HE\]](https://arxiv.org/abs/2306.16213).
- [80] G. Agazie *et al.* (NANOGrav), The NANOGrav 15 yr Data Set: Constraints on Supermassive Black Hole Binaries from the Gravitational-wave Background, *Astrophys. J. Lett.* **952**, L37 (2023), [arXiv:2306.16220 \[astro-ph.HE\]](https://arxiv.org/abs/2306.16220).
- [81] J. Antoniadis *et al.* (EPTA, InPTA:), The second data release from the European Pulsar Timing Array - III. Search for gravitational wave signals, *Astron. Astrophys.* **678**, A50 (2023), [arXiv:2306.16214 \[astro-ph.HE\]](https://arxiv.org/abs/2306.16214).
- [82] J. Antoniadis *et al.* (EPTA), The second data release from the European Pulsar Timing Array: V. Implications for massive black holes, dark matter and the early Universe, (2023), [arXiv:2306.16227 \[astro-ph.CO\]](https://arxiv.org/abs/2306.16227).
- [83] D. J. Reardon *et al.*, Search for an Isotropic Gravitational-wave Background with the Parkes Pulsar Timing Array, *Astrophys. J. Lett.* **951**, L6 (2023), [arXiv:2306.16215 \[astro-ph.HE\]](https://arxiv.org/abs/2306.16215).
- [84] H. Xu *et al.*, Searching for the Nano-Hertz Stochastic Gravitational Wave Background with the Chinese Pulsar

- Timing Array Data Release I, *Res. Astron. Astrophys.* **23**, 075024 (2023), [arXiv:2306.16216 \[astro-ph.HE\]](#).
- [85] C. A. R. Herdeiro and E. Radu, Kerr black holes with scalar hair, *Phys. Rev. Lett.* **112**, 221101 (2014), [arXiv:1403.2757 \[gr-qc\]](#).
- [86] C. Herdeiro, E. Radu, and H. Rúnarsson, Kerr black holes with Proca hair, *Class. Quant. Grav.* **33**, 154001 (2016), [arXiv:1603.02687 \[gr-qc\]](#).
- [87] E. Babichev and C. Deffayet, An introduction to the Vainshtein mechanism, *Class. Quant. Grav.* **30**, 184001 (2013), [arXiv:1304.7240 \[gr-qc\]](#).
- [88] O. J. C. Dias, J. E. Santos, and B. Way, Numerical Methods for Finding Stationary Gravitational Solutions, *Class. Quant. Grav.* **33**, 133001 (2016), [arXiv:1510.02804 \[hep-th\]](#).



## SUPPLEMENTAL MATERIAL

### Numerical method

In our numerical setup, we utilize the compactified radial coordinate  $x = 1 - 2\rho_H/\rho$ , which maps the interval  $[\rho_H, \infty[$  to  $[-1, 1]$ . The boundary conditions we impose are as follows: at the horizon ( $x = -1$ ), our functions obey  $f - 2\partial_x f = g + 2\partial_x g = \partial_x \phi = \partial_x \psi = 0$ . To ensure asymptotic flatness, we impose that  $f = g = h = 1$ , and  $\phi = \psi = 0$  at  $x = 1$ . To solve the differential-algebraic system resulting from the field equations (2), (3) and (4), our code employs a pseudospectral method together with the Newton-Raphson root-finding algorithm (see Refs. [52, 88]). We expand each of the functions in a spectral series with resolution  $N_x$  in the radial coordinate  $x$ . The spectral series we use for each of the functions  $\mathcal{F}^{(k)} = \{f, g, \phi, \psi\}$  is given by

$$\mathcal{F}^{(k)} = \sum_{i=0}^{N_x-1} \alpha_i^{(k)} T_i(x), \quad (\text{i})$$

where  $T_i(x)$  denotes the  $i$ -th Chebyshev polynomial, and  $\alpha_i^{(k)}$  are the spectral coefficients of the  $k$ -th function. We have typically used a resolution  $N_x \sim 40$ .

From the physical quantities of the solutions, we can estimate the accuracy of the numerical solutions using a Smarr-type relation they should obey

$$M = 2T_H S + \frac{1}{4\pi} \int d^3x \sqrt{-g} F(\phi) \left[ \frac{\square\phi}{F'(\phi)} + \alpha_2^3 \psi^2 \right], \quad (\text{ii})$$

where  $T_H = \frac{1}{2\pi\rho_H} \frac{f}{\sqrt{g}}|_{\mathcal{H}}$  is the Hawking temperature of the solutions. We assessed the numerical accuracy of our solutions through multiple approaches. Firstly, we considered Eq. (ii), recognizing that it is susceptible to numerical errors due to numerical integration. Additionally, we examined the order of magnitude of the last retained spectral coefficient, and the minimization of the residuals. In general, the Smarr relation yielded errors on the order of  $\mathcal{O}(10^{-8})$ . However, as we approached the end of the existence domain for scalarized solutions with sufficiently large couplings, errors increased to around  $\mathcal{O}(10^{-4})$ . This error pattern aligns with what is observed with our code in the standard scalar-Gauss-Bonnet case, where it underwent thorough testing [27, 52] and faithfully reproduced results from the existing literature [9–12]. The last retained spectral coefficient typically yielded an error estimate approximately a few orders of magnitude smaller than that of the Smarr relation, while the norm of the residuals consistently dropped below  $\mathcal{O}(10^{-10})$ . Finally, we observed that the bifurcation points from Schwarzschild, for each value of  $\alpha_2/\alpha_1$ , agree with high-accuracy with the upper bound values derived from the S-deformation method, providing a final test to the code.

### Physical quantities of interest of scalarized solutions

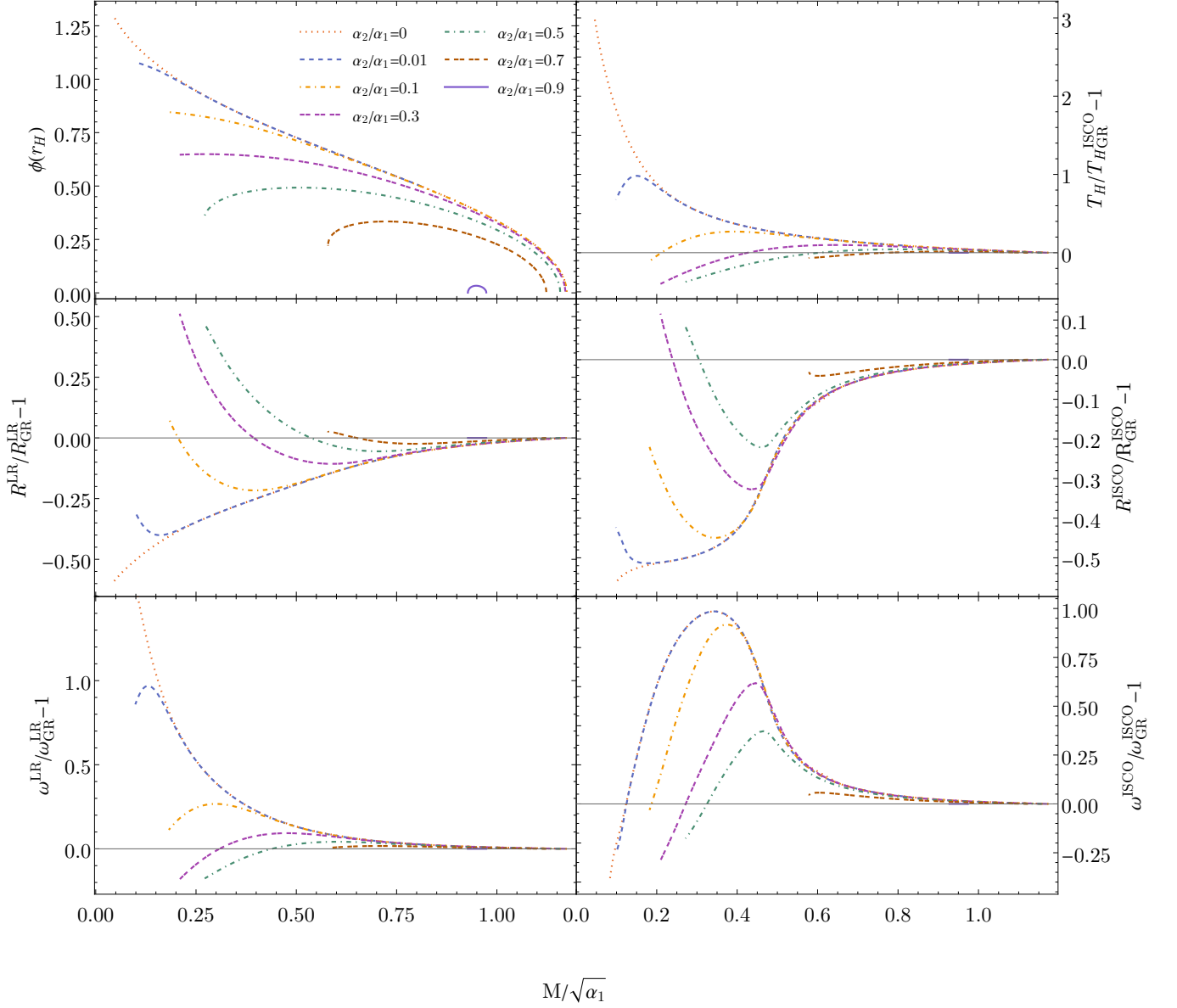


FIG. 4. Physical quantities characterizing scalarized solutions for a selection of  $\alpha_2/\alpha_1$  values. Progressing from left to right and top to bottom, these include: the value of  $\phi$  at the horizon, the Hawking temperature, the perimetral location of the light ring, perimetral location of the innermost stable circular orbit (ISCO), the geodesic frequency at the light ring, and the geodesic frequency at the ISCO. With the exception of the value of  $\phi$  at the horizon, we compare all quantities to those of an equivalent Schwarzschild black hole.